Journal of Applied Electrochemistry
https://doi.org/10.1007/s10800-023-02009-4

RESEARCH ARTICLE

Electrochemical and physiochemical studies on the effects of thiadiazole derivatives in corrosion inhibition of Muntz metal in sulfide-polluted marine environment

Parkavi Ravisankar[1] · Jayavel Murugasamy[1] · Sivasankaran Ayyaru[2] · Srinivasan Kanagaraj[3] · Jagadeesh Kumar Alagarasan[4] · Imran Hasan[5] · Prathap Somu[6] · Akhilesh Kumar Yadav[7,8,9] · Young-Ho Ahn[2]

Received: 21 May 2023 / Accepted: 15 October 2023

Abstract

The influence of certain thiadiazole derivatives on the corrosion of Muntz metal (60Cu–40Zn) in sulfide-polluted artificial seawater was analyzed using electrochemical and physiochemical studies methods. The surface morphology was examined by SEM to determine this inhibition mechanism. Elemental composition of the corroded alloy specimens was investigated in the presence and absence of thiadiazole derivatives using energy-dispersive X-ray analysis (EDX). Thiadiazole derivatives were found to successfully suppress Muntz metal corrosion. Adopting the weight loss method, the optimum concentration of inhibiting thiadiazole derivatives was 2.32 mM owing to the thiadiazole surface coverage and adsorption with increasing concentration. Among the derivatives investigated, N-(5-(4-aminophenyl)-1,3,4-thiadiazole-2-yl)-2-diphenylamino) acetamide (ATPA) showed the highest corrosion protection efficiency. EIS studies showed that charge transfer resistance occurs because of the presence of an inhibitor. Moreover, increasing thiadiazole concentration decreased the double-layer capacitance (C_{dl}) value because less charged species were attracted to the metal surface. Potentiostatic current–time transient techniques showed that ATPA hindered the corrosion rate owing to the substituted thiadiazoles. Polarization measurements clearly showed that the inhibitors suppressed both anodic and cathodic reactions. Consequently, accelerated leaching studies showed concentrations of Zn and Cu released from the alloy reducing as concentrations of inhibitors increased, in addition to the corrosion protection efficiency (%) increasing. The highest value was obtained at 2.32 mM of inhibitor. In conclusion, this study demonstrates that these compounds inhibit corrosion via chemisorption of organic compounds. Among these compounds, ATPA was found to offer better corrosion inhibition than others.

Parkavi Ravisankar and Jayavel Murugasamy have contributed equally to this work.

✉ Sivasankaran Ayyaru
sivasankaran2010@gmail.com

✉ Akhilesh Kumar Yadav
yadavbasti@gmail.com

✉ Young-Ho Ahn
yhahn@ynu.ac.kr

[1] Department of Chemistry, Meenakshi College of Engineering, West K. K. Nagar, Chennai, Tamil Nadu 600078, India

[2] Department of Civil Engineering, Yeungnam University, Gyeongsan 38541, Republic of Korea

[3] Department of Botany, Vivekananda College, Agasteeswaram, Kanyakumari, Tamil Nadu 629701, India

[4] Department of Bioengineering, Saveetha School of Engineering, Saveetha Institute of Medical and Technical Science, Chennai 602105, India

[5] Department of Chemistry, College of Science, King Saud University, Riyadh 11451, Saudi Arabia

[6] Department of Biotechnology and Chemical Engineering, School of Civil & Chemical Engineering, Manipal University Jaipur, Dehmi Kalan, Off. Jaipur-Ajmer Expressway, Jaipur, Rajasthan 303007, India

[7] Department of Environmental Engineering and Management, Chaoyang University of Technology, Taichung 413310, Taiwan

[8] Environmental Science and Engineering Department, Indian Institute of Technology Bombay, Mumbai 400076, India

[9] Department of Mining Engineering, Indian Institute of Technology (Banaras Hindu University), Varanasi 221005, India

Published online: 15 November 2023

Graphical abstract

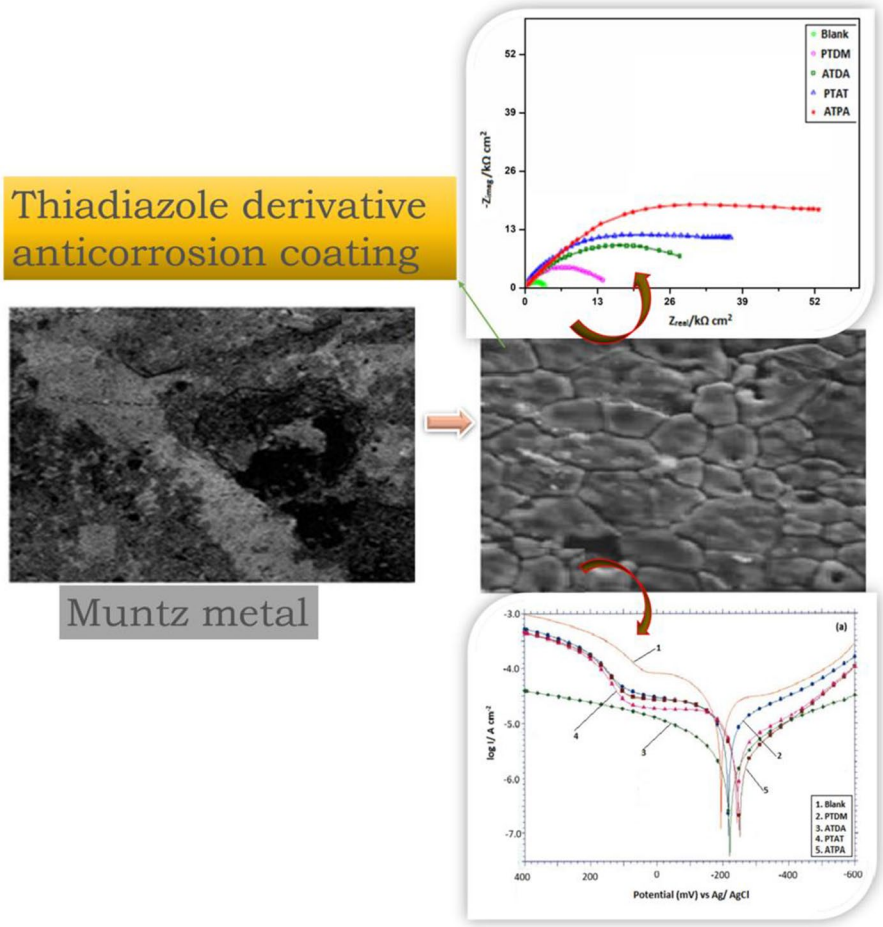

Keywords Corrosion inhibitor · Thiadiazole derivatives · Dezincification · Muntz metal

1 Introduction

Organic inhibitors are among the most important materials for corrosion prevention and control [1–3]. Cu–Zn alloys (brasses) may suffer significant corrosion issues, particularly because of continuous exposure to aerated water rich in carbon dioxide or chloride ions. [4, 5]. Brasses exhibit low corrosion resistance due to the phenomenon of dezincification in specific environments [6–8]. From an electrochemical standpoint, the phenomenon of dezincification in Muntz metal can be attributed to the higher electrochemical activity and relatively greater nobility of zinc compared to copper. This significant disparity in electrochemical potential between copper and zinc results in zinc exhibiting a substantial overpotential for selective dissolution, contributing to the process of dezincification [9]. Heat exchangers, condensers, and fluid control devices have been widely constructed using copper- and copper-based alloys. Additionally, the alloys are utilized in architectural components, building fronts, railways, lock bodies, doorknobs, electrical wiring, hardware, connections, printed circuit boards, and electronic applications [3, 4, 10]. Drach et al. (2013) studied the corrosion behavior of alpha plus beta brasses in seawater environments, focusing on the role of alloy composition in determining their corrosion resistance. The research highlighted the significance of the alpha and beta phase fractions in influencing the overall corrosion performance of these alloys [11]. Numerous strategies have been developed to reduce corrosion-related losses. The minimization of corrosion of copper and its alloys in water transport systems, by alloying and incorporating inhibitors, has been extensively studied [12, 13].

Protecting metals and alloys against attacks in many industrial environments requires the addition of inhibitors [14, 15]. Corrosion is a severe issue for the service life of alloys used in industry. Thus, the development of corrosion

inhibitors based on organic compounds containing nitrogen, sulfur, and oxygen atoms is of growing importance on the subject of corrosion and industrial chemistry [16, 17]. Heterocyclic organic inhibitors that contain nitrogen, sulfur, and oxygen atoms, mostly azoles such as triazoles, thiazoles, thiadiazoles, imidazoles, etc., are frequently used to protect metals and alloys from corrosion [18–24]. Thus, most organic molecules contain heteroatoms which serve as effective inhibitors. However, the stability and corrosion efficiency of these inhibitors are more critical [25, 26]. According to previous research, effective inhibitors should have several π-electrons and unshared electron pairs on either their nitrogen or sulfur atoms, compared to the d-orbital of iron [27, 28]. Thiadiazole derivatives contain sulfur atoms in their moiety and offer unshared electron pairs. Al-Amiery et al. (2019) investigated the corrosion inhibition potential of various thiadiazole derivatives on mild steel in hydrochloric acid environments. Their work emphasized the importance of electron-rich sulfur and nitrogen atoms in the inhibitors' structures, which contributed to the formation of protective adsorbed layers on the metal surface. Zhang et al. (2020) investigated the corrosion inhibition potential of newly synthesized thiadiazole derivatives on carbon steel in a saline environment. Their research emphasized the correlation between the molecular structure of the inhibitors and their adsorption behavior on the metal surface [29]. Therefore, this finding creates greater interest in investigating thiadiazole derivatives as corrosion inhibitors for Muntz metals.

In the present work, the influence of certain thiadiazole derivatives, namely N-(5-phenyl-1,3,4-thiadiazol-2-yl)acetamide (PTDM), N-(5-(4-aminophenyl)-1,3,4-thiadiazole-2-yl)-2-(diethylamino) acetamide (ATDA), 2-(5-phenyl-1,3,4-thiadiazol-2-ylamino)-N-p-tolyl acetamide (PTAT) and N-(5-(4-aminophenyl)-1,3,4-thiadiazole-2-yl)-2-diphenylamino)acetamide (ATPA) on the corrosion of Muntz metal (60Cu–40Zn) in sulfide-polluted artificial seawater has been analyzed by electrochemical and physiochemical methods. The surface morphological study was carried out using SEM analysis to determine the mechanism of corrosion inhibition. The elemental composition of the corroded alloy specimen was investigated in the presence and absence of thiadiazole derivatives using energy-dispersive X-ray analysis (EDX).

2 Materials and methods

2.1 Preparation of sulfide-polluted marine water (artificial)

Marine water was prepared artificially by introducing chemicals into a liter of distilled water, as given in Table 1S [30]. A stock solution of sulfide-polluted artificial seawater was prepared by dissolving 2.44 g of analytical grade Na_2S in 1 L of artificial seawater in a standard measuring flask [31]. Thiadiazole derivatives PTDM, ATDA, PTAT, and ATPA were synthesized as per the previously reported procedures in the literature [28, 29]. The structures of the thiadiazole derivatives are given in Table 1.

2.2 Corrosion protection studies

The corrosion protection performance of thiadiazoles on Muntz metal in sulfide-polluted artificial seawater was

Table 1 Structures of the thiadiazole derivatives

Name	Abbreviation	Structure
N-(5-phenyl-1,3,4-thiadiazol-2-yl)acetamide	PTDM	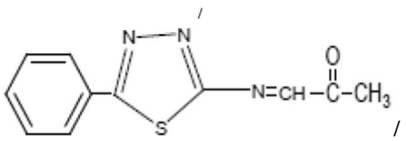
N-(5-(4-aminophenyl)-1,3,4-thiadiazole-2-yl)-2-(diethyl amino) acetamide	ATDA	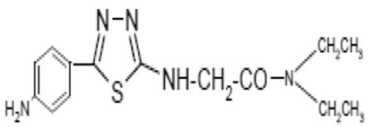
2-(5-phenyl-1,3,4-thiadiazol-2-ylamino)-N-ptolylacetamide	PTAT	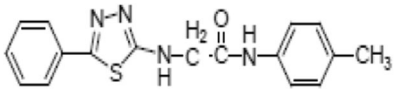
N-(5-(4-aminophenyl)-1,3,4-thiadiazole-2-yl)-2-(diphenylamino)acetamide	ATPA	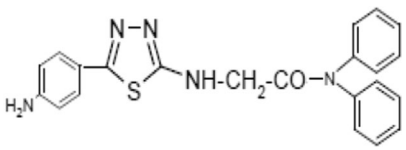

investigated using chemical methods, such as the weight loss method, and electroanalytical methods, such as potentiodynamic polarization, electrochemical impedance spectroscopy, potentiostatic current–time transient, and ICP-AES studies. The surface characterization of the corroded Muntz metal samples was examined by scanning electron microscopy (SEM) analysis and energy-dispersive X-ray (EDX).

2.2.1 Specimen preparation

The Muntz metal (brass alloy (Cu 60/Zn 40)) was the scope material for this study. Muntz metal alloy samples were cut into plain 4 cm × 3 cm × 0.3 cm sizes for the weight loss method. For each electrochemical study, Muntz metal alloy specimens were cut into overall 1 cm^2 sizes and embedded in araldite (thermosetting polymer) with an electrical connection, leaving an exposed area of 1 cm^2. Before each experiment, the Muntz metal sample was polished using various grades of silicon carbide sheets, (80–1000 grit), washed with distilled water, degreased ultrasonically with acetone, and air-dried.

2.2.2 Weight loss measurements

Weight loss measurements were performed for a duration of 5 days. A small hole was made near the top edge of the Muntz metal specimen to suspend it in the test solution. The Muntz metal alloy specimens were mechanically polished successively to the required dimensions with different grits of silicon carbide papers. Double-distilled water was used to wash the polished Muntz metal specimens, which were ultrasonically cleaned with acetone. After recording their initial weight, the Muntz metal alloy specimens were suspended in 500-ml beakers containing 250 ml of sulfide-polluted artificial seawater with and without different concentrations of thiadiazole derivatives at a temperature of 30 °C. After a defined immersion time, the specimens were removed, cleaned under running water, and dried and the weight changes were noted. The corrosion rate (CR) and percent corrosion protection efficiencies were determined using the following equations [32]:

$$\text{CR (mils/year)} = \frac{534 \times W}{D \times A \times t} \tag{1}$$

$$\text{IE\%} = \frac{\text{CR}_{(\text{bl})} - \text{CR}_{(\text{inh})}}{\text{CR}_{(\text{bl})}} \times 100 \tag{2}$$

where W is the weight loss (mg), D is the density of the Muntz metal alloy (g cm^{-3}), A is the area of the specimen ($inch^2$), and t is the immersion time (h). $CR_{(bl)}$ and $CR_{(inh)}$ are the corrosion rates of Muntz metal in the absence and presence of corrosion inhibitors, respectively.

2.3 Electrochemical studies

2.3.1 Electrochemical cell assembly

The general electrochemical setup used for all electrochemical studies, namely potentiodynamic polarization, electrochemical impedance spectroscopy, and potentiostatic current–time transient techniques, consisted of a 400-ml flat-bottomed flask equipped with platinum foil as the counter electrode, Ag/AgCl in saturated potassium chloride (KCl) as the reference electrode, and Muntz metal with an exposed area of 1 cm^2 as the working electrode. All electrochemical studies were performed in the present research using an electrochemical workstation (CHI 760, CH Instruments, USA).

2.3.2 Potentiodynamic polarization studies

Tafel polarization measurements were performed using a specimen of Muntz metal alloy with an area of 1 cm^2. The working electrode (the Muntz metal specimen) was then immersed in an aqueous chloride environment, polarized at −1.0 V (Ag/AgCl) for 20 min to reduce all oxides on the alloy surface, and then allowed to stabilize for 30 min [26]. The Tafel polarization curves of the Muntz metal alloy specimens in sulfide-polluted artificial seawater with and without different concentrations of the azole derivatives (pyrazole, thiadiazole, and benzotriazole) were recorded at a scan speed of 1 mV s^{-1}.

The corrosion protection efficiencies of the inhibitors were calculated using I_{corr} values. The corrosion rate (mils/year) and corrosion inhibition efficiency (%) were calculated using the following equations [33, 34]:

$$\text{CR (mils/year)} = \frac{0.129 \times \text{I}_{\text{corr}} \times \text{Eq.W}}{\rho} \tag{3}$$

$$\text{PE}(\%) = \frac{\text{I}_{\text{corr}} - \text{I}_{\text{corr (inh)}}}{\text{I}_{\text{corr}}} \times 100 \tag{4}$$

where ρ is the density (g cm^{-3}), Eq. W is the equivalent weight of the specimen, CR is the corrosion rate (mils/year), and PE is the protection efficiency. I_{corr} and $I_{corr(inh)}$ are the corrosion current densities in the absence and presence of the inhibitors, respectively.

2.3.3 Potentiostatic current–time transient techniques

This test may have been necessary because seawater contains large amounts of chloride and oxygen and often exhibits the most dramatic dealloying of brass [3, 35, 36]. The potentiostatic current–time transients of the Muntz

metal alloy in sulfide-polluted artificial seawater with and without different concentrations of pyrazole, thiadiazole, and benzotriazole derivatives were recorded at different potentials (−200, −160, −120, −80, −40, and 0 mV).

2.3.4 Accelerated leaching studies by ICP-AES

After polarization measurements, the test solutions with and without different concentrations of the thiadiazole derivatives were collected, and the concentrations of Cu and Zn leached out from the alloy were determined by ICP-AES. The dezincification index was determined using the following equation [37]:

$$z = \frac{([Zn]\ /[Cu])_{soln}}{([Zn]/[Cu])_{alloy}}$$

where $[Zn]_{soln}$ and $[Zn]_{alloy}$ are the concentrations of zinc in the solution and alloy, respectively. Similarly, $[Cu]_{sol}$ and $[Cu]_{alloy}$ are the concentrations of copper in the solution and alloy, respectively.

2.3.5 Scanning electron microscopy (SEM)

SEM is a valuable method for analyzing the morphology of corroded surfaces of metals and alloys. In scanning electron microscopy, the metal/alloy specimen is scanned with a fixed electron beam that traces a line raster pattern. This technique is characteristic of all electron probe-scanning instruments. There is a point-to-point match between the target and the image in a few instances. The working electrode (Muntz metal) was immersed in artificially prepared sulfide-polluted seawater containing optimal concentrations of substituted azole derivatives for 120 h, and the surface of the Muntz metal was observed using a scanning electron microscope (SEM; Model: JEOL JSM-6390LV/LGS).

2.3.6 Energy-dispersive X-ray analysis (EDX)

EDX Spectrometry uses the X-ray spectrum emitted by a solid sample bombarded with a fixed beam of electrons to obtain a localized chemical analysis. EDX analysis is very potent, especially for pollution analysis and modern forensic science research. The Muntz metal was immersed in sulfide-polluted seawater containing optimal concentrations of substituted azoles for 72 h. After that, the Muntz metal was removed, thoroughly washed with double-distilled water, cleaned with acetone, and then dried. Energy-dispersive X-ray analysis was carried out using an EDX analyzer (JEOL Model JED-2300, Energy-Dispersive X-ray Analyzer USA).

3 Results and discussion

3.1 Weight loss measurements

All the synthesized substituted thiadiazole derivatives, PTDM, ATDA, PTAT, and ATPA were tested at four different concentrations (0.76, 1.54, 2.32, and 3.07 mM) for analyzing the protective effect of Muntz metal in

Table 2 Calculated values of weight loss, corrosion rate, and corrosion protection efficiency for Muntz metal in sulfide-polluted artificial seawater for various concentrations of PTDM, ATDA, PTAT, and ATPA at 303 K

Thiadiazole derivatives	Conc. of thiadiazole derivatives (mM)	Weight loss (mg)	Corrosion rate (mils year^{-1})	Inhibition efficiency (%)
Blank	0	76.29	10.34	–
PTDM	0.76	32.61	4.42	57.25
	1.54	21.91	2.97	71.28
	2.32	5.46	0.74	92.84
	3.07	5.98	0.81	92.17
ATDA	0.76	28.33	3.84	62.86
	1.54	17.49	2.37	77.08
	2.32	4.13	0.56	94.58
	3.07	4.35	0.59	94.29
PTAT	0.76	24.42	3.31	67.99
	1.54	17.56	2.38	76.98
	2.32	2.29	0.31	97.00
	3.07	2.51	0.34	96.71
ATPA	0.76	18.30	2.48	76.02
	1.54	11.95	1.62	84.33
	2.32	0.81	0.11	98.94
	3.07	0.96	0.13	98.74

sulfide-polluted artificial seawater, and the related weight loss data are given in Table 2. The table shows that, as the concentration (0.76, 1.54, 2.32, and 3.07 mM) of thiadiazole derivatives PTDM, ATDA, PTAT, and ATPA increases, the corresponding weight loss decreases to 2.3 mg and further down. The optimum concentration of the inhibiting thiadiazole derivatives was found to be 2.32 mM. The substituted thiadiazoles increased the surface coverage and adsorption as the concentration increased, distinctly separating the alloy's surface from the chloride environment. Table 2 shows that PTDM, ATDA, PTAT, and ATPA competently reduced the alloy's weight loss and corrosion rate, increasing their inhibiting protection efficiencies and reaching the highest concentration value of 2.32 mM. The weight loss in the absence of a corrosion inhibitor was 76.29 mg in sulfide-polluted artificial seawater, and it was decreased by the addition of 2.32-mM concentrated PTDM, ATDA, PTAT, and ATPA to lower values 5.46, 4.13, 2.29, and 0.81 mg, respectively.

In sulfide-polluted artificial seawater, the corrosion rate of Muntz metal is 10.34 mils/year. It is reduced by adding 2.32 mM (the optimum concentration) of thiadiazole derivatives PTDM, ATDA, PTAT, and ATPA to a lower value of 0.74 0.56, 0.34, and 0.11 mils yr^{-1}, respectively.

With an increase in concentration up to 2.32 mM, the corrosion protection effectiveness of PTDM, ATDA, PTAT, and ATPA increased, and the protection efficiency slightly decreased. This was due to the interaction between the absorbed thiadiazole molecules on the surface of the Muntz metal sites. The degree of corrosion protection efficiency was based on the concentration and nature of PTDM, ATDA, PTAT, and ATPA. The optimum concentration was determined using the corrosion protection efficiency of PTDM, ATDA, PTAT, and ATPA, and it was found to be 2.32 mM for all four inhibitors. In sulfide-polluted artificial seawater, the thiadiazole derivatives PTDM, ATDA, PTAT, and ATPA showed maximum inhibition efficiencies of 92.84, 94.58, 97.0, and 98.94%, respectively, at their optimum concentrations. Among the thiadiazole derivatives investigated, ATPA showed the highest corrosion inhibition efficiency for the Muntz metal in sulfide-polluted artificial seawater. Figure 1 shows the variation in corrosion rate (mils/year) of Muntz metal in sulfide-polluted artificial seawater with and without different concentrations (0.76, 1.54, 2.32, and 3.07 mM) of substituted thiadiazole derivatives PTDM, ATDA, PTAT, and ATPA. As shown in Fig. 1, the corrosion rate decreased with increasing concentration of thiadiazole derivatives. This trend may be a result of the adsorption and surface coverage increase with increasing concentration; thus, the alloy surface is proven to be perfectly separated from the aqueous chloride environment.

The solubility of thiadiazole derivatives, specifically PTDM, ATDA, PTAT, and ATPA, as inhibitors in sulfide-polluted artificial seawater is a topic of significant interest.

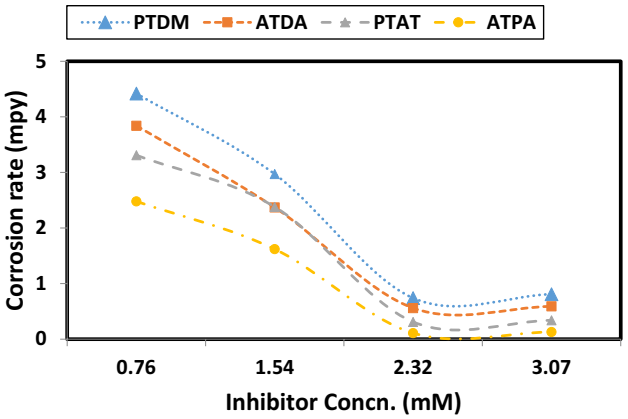

Fig. 1 Effect of various concentrations of PTDM, ATDA, PTAT, and ATPA on the corrosion rate of Muntz metal in sulfide-polluted artificial seawater

ATPA, in particular, is known to be poorly soluble in this environment but shows remarkable productivity when used in the context of Muntz metal corrosion inhibition. This phenomenon raises questions about the formation of protective films on the surface of Muntz metal. Such films may potentially hinder the interfacial contact between the metal ions (Muntz metal) and the inhibitors containing organic molecules. In this context, these protective films primarily depend on the nature of the organic molecules involved. They typically have hydrophilic groups that bond with the metal surface and hydrophobic groups that interact with the surrounding seawater. In the case of thiadiazole derivatives, such as ATDA, the adsorbed inhibitor molecules play a crucial role in limiting the diffusion of oxygen and preventing seawater access to the metal surface. This action, in turn, leads to a reduction in the corrosion rate and an increase in the inhibition efficiency of the thiadiazole derivatives.

3.2 Electrochemical impedance spectroscopic studies

We conducted a comprehensive analysis using electrochemical impedance spectroscopy to investigate the behavior of Muntz metal in sulfide-polluted artificial seawater with varying concentrations of thiadiazole derivatives. The relevant impedance parameters are documented in Table 3. In Fig. 2, we present the electrochemical impedance diagrams represented in the Nyquist plot. These diagrams were obtained at the open-circuit potential region after immersing the Muntz metal specimens for 1 h in sulfide-polluted artificial seawater, both with and without the optimum concentrations of thiadiazole derivatives. We observed a notable trend in the charge transfer resistance values, which are detailed in the tables. Initially, with increasing concentrations of thiadiazole derivatives, namely PTDM, ATDA, PTAT, and ATPA,

Table 3 Values of charge transfer resistance, double-layer capacitance, faradaic resistance, faradaic capacitance, and inhibition efficiency for Muntz metal in sulfide-polluted artificial seawater at different concentrations of PTDM, ATDA, PTAT, and ATPA

Thiadiazole derivatives	Conc. of thiadiazole derivatives (mM)	RF (Ω cm^{-2}) × 104	CF (μF cm^{-2})	Cdl (μF cm^{-2})	Rct (Ω cm^{-2}) × 104	Inhibition efficiency (%)
Blank	0	0.862	35.18	37.56	0.712	–
PTDM	0.76	3.345	18.65	17.53	2.962	75.96
	1.54	7.271	4.743	4.462	6.823	89.56
	2.32	14.27	0.976	1.143	13.78	94.83
	3.07	14.22	0.979	1.150	13.64	94.78
ATDA	0.76	3.856	15.67	14.52	3.561	80.05
	1.54	8.932	3.482	3.021	8.482	91.61
	2.32	17.05	0.834	0.762	16.79	95.76
	3.07	17.01	0.836	0.765	16.64	95.72
PTAT	0.76	5.234	11.78	9.145	4.824	85.24
	1.54	10.78	3.367	2.987	10.37	93.14
	2.32	20.43	0.643	0.581	19.83	96.41
	3.07	20.40	0.648	0.584	19.80	96.04
ATPA	0.76	6.932	6.215	3.648	6.461	88.98
	1.54	13.47	1.632	0.965	13.02	94.53
	2.32	23.94	0.487	0.325	23.21	96.93
	3.07	23.88	0.490	0.328	23.12	96.92

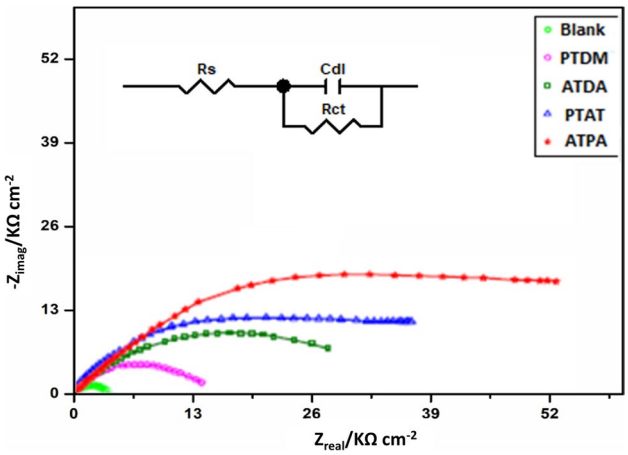

Fig. 2 Impedance diagram and equivalent circuit of Muntz metal in a solution containing an optimum concentration of PTDM, ATDA, PTAT, and ATPA sulfide-polluted artificial seawater

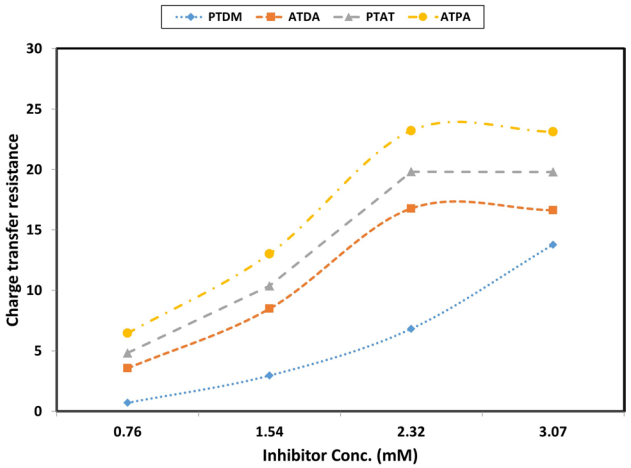

Fig. 3 Plot of charge transfer resistance vs. different concentrations of PTDM, ATDA, PTAT and ATPA for Muntz metal in sulfide-polluted artificial seawater

the charge transfer resistance values showed an increase, reaching a peak at 2.32 mM. Subsequently, there was a slight decrease, and we did not observe any significant further increase in Rct values. To illustrate this trend more comprehensively, we have depicted the charge transfer resistance as a function of different concentrations of PTDM, ATDA, PTAT, and ATPA for Muntz metal in sulfide-polluted artificial seawater in Fig. 3.

For context, when no inhibitor was present, the charge transfer resistance value for Muntz metal in sulfide-polluted artificial seawater was 0.712×104 Ω cm^{-2}. Upon the addition of the optimal concentration (2.32 mM) of PTDM, ATDA, PTAT, and ATPA, we observed a significant increase in resistance. The values reached 13.78×104, 16.79×104, 19.83×104, and 23.21×104 Ω cm^{-2}, respectively (as depicted in Fig. 3). Notably, the presence of inhibitors resulted in the formation of a substantial semicircle in the Nyquist plots, extending from high to low frequencies. This observation underscores the dominant influence of charge transfer resistance during the corrosion process, which is

attributed to the formation of a protective thiadiazole film on the surface of Muntz metal.

Electrochemical impedance spectroscopic analyses were conducted for Muntz metal in sulfide-polluted artificial seawater containing various concentrations of thiadiazole derivatives; their appropriate impedance parameters are provided in Table 3. The electrochemical impedance diagrams given in the Nyquist plot obtained at the region of open-circuit potential when Muntz metal was immersed (1 h) in sulfide-polluted artificial seawater with and without the presence of optimum concentrations of thiadiazole derivatives are presented in Fig. 2. The charge transfer resistance values in the tables were observed to have increased with increasing concentration of the thiadiazole derivatives PTDM, ATDA, PTAT, and ATPA up to 2.32 mM, then slightly decreased, and no significant increase in R_{ct} values was noted. The charge transfer resistance vs. different concentrations plot of PTDM, ATDA, PTAT, and ATPA for Muntz metal in sulfide-polluted artificial seawater is shown in Fig. 3.

The charge transfer resistance values of the Muntz metal in the absence of an inhibitor in sulfide-polluted artificial seawater was $0.712 \times 104\ \Omega\ cm^{-2}$. It was increased by the addition of the optimum concentration (2.32 mM) of PTDM, ATDA, PTAT, and ATPA to a maximum value of 13.78×104, 16.79×104, 19.83×104, and $23.21 \times 104\ \Omega\ cm^{-2}$, respectively (Fig. 3). The large semicircle observed from high to low frequencies in the presence of the inhibitor indicates that the charge transfer resistance dominated during the corrosion process owing to the formation of a thiadiazole film on the Muntz metal surface.

The double-layer capacitance (C_{dl}) values of Muntz metal in sulfide-polluted artificial seawater decreased with increasing PTDM, ATDA, PTAT, and ATPA concentrations. As the local dielectric constant decreased and the strength of the electrical double layer increased, they indicated that the thiadiazole derivatives adsorbed well at the metal–solution interface. In the absence of thiadiazole derivatives in sulfide-polluted artificial seawater, the double-layer capacitance (C_{dl}) value was 37.56 μF cm^{-2}. It was decreased by the addition of PTDM, ATDA, PTAT, and ATPA, at the optimum concentration (2.32 mM), to a minimum value of 1.143, 0.762, 0.581, and 0.325 μF cm^{-2}, respectively. As an inhibitor was adsorbed, the decreased excess of charged species on the Muntz metal surface created a good permanent layer on the alloy surface, causing a decrease in the C_{dl} value and an increase in thiadiazole concentration. The variation in R_{ct} and C_{dl} values was caused by the gradual replacement of H_2O molecules by Cl^- ions present in the chloride medium, and the adsorption of the thiadiazole molecules on the Muntz metal surface, which decreased the degree of dissolution.

In sulfide-polluted artificial seawater, PTDM, ATDA, PTAT, and ATPA exhibited maximum protection efficiencies of 94.83, 95.76, 96.41, and 96.93%, respectively, at their optimum concentration. Among the thiadiazole derivatives assessed, ATPA showed the highest corrosion protection of the Muntz metal in a sulfide-polluted artificial seawater environment.

The faradaic resistance (R_F) values increased with the concentration of the thiadiazole derivatives PTDM, ATDA, PTAT, and ATPA, showing that the inhibitor sustains the corrosion material over the Muntz metal. When the strength of PTDM, ATDA, PTAT, and ATPA increased, the R_F values and faradaic values decreased because the organic compounds adsorbed well on the Muntz metal surface.

Molecular structure inhibitors usually define adsorption on a Muntz metal surface. Thiadiazole derivatives such as PTDM, ATDA, PTAT, and ATPA showed variation in their protection efficiencies due to their dissimilar molecular arrangements. ATPA had the highest corrosion inhibition efficiency compared to the other thiadiazole derivatives, which was in accordance with the weight loss measurements. The inhibition efficiency (%) calculated by impedance studies showed the same trend as that seen in weight loss sizes, which is, interrelated weight loss measurements and electrochemical impedance.

3.3 Potentiostatic current–time transient techniques

Potentiostatic current–time transient assessments were carried out at several impressed potentials (−200, −160, −120, −80, −40, and 0 mV) compared to SCE, anodic to the corrosion potential (E_{corr}) of Muntz metal in sulfide-polluted artificial seawater containing the optimum concentration (2.32 mM) of thiadiazole derivatives, namely PTDM, ATDA, PTAT, and ATPA. The illustrative curves are presented in Fig. 4**.** The current density values of the Muntz metal in sulfide-polluted artificial seawater in the presence and absence of thiadiazole derivatives PTDM, ATDA, PTAT, and ATPA attained at various impressed potentials are given in Table 4. From this table, the investigated thiadiazole derivatives were observed to strongly decrease in current density values and thus effectively reduce the rate of corrosion of Muntz metal in a chloride environment. The current density values of Muntz metal in sulfide-polluted artificial seawater in the absence of thiadiazole derivatives, at different impressed potentials of −200, −160, −120, −80, −40, and 0 mV, respectively, were 0.096, 0.51, 1.32, 2.47, 4.13, and 5.68 mA cm^{-2}. The compound N-(5-(4-aminophenyl)-1,3,4-thiadiazole-2-yl)-2-diphenylamino) acetamide (APTD) competently decreased the current density values of 0.015, 0.062, 0.19, 0.48, 1.35, and 1.84 and thus controls corrosion of Muntz metal in an artificial seawater environment, as displayed in Table 4. The I_{corr} values obtained in this analysis highlight the interpretation made

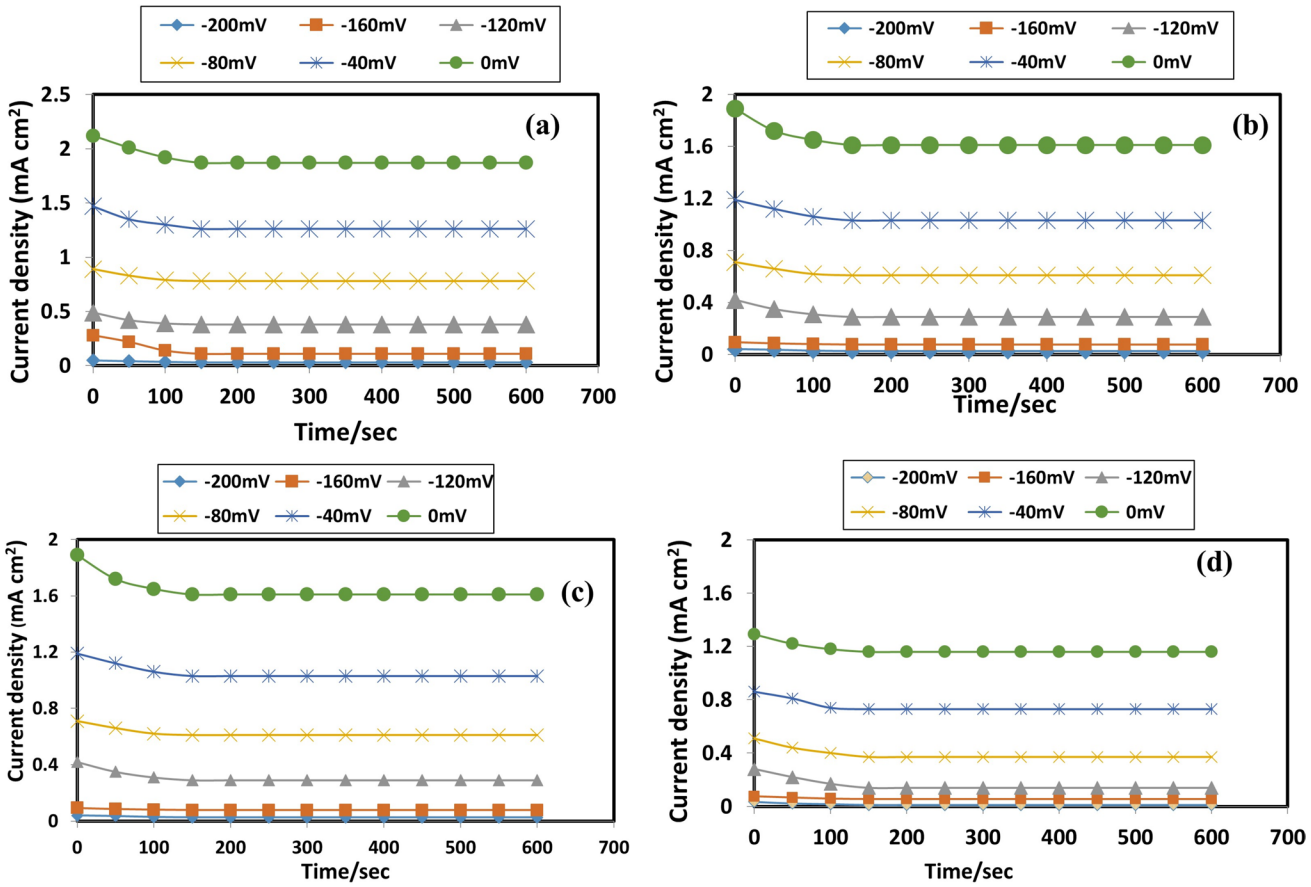

Fig. 4 Potentiostatic current–time transient curves of Muntz metal in sulfide-polluted artificial seawater containing optimum concentration of **a** PTDM, **b** ATDA, **c** PTAT, and **d** ATPA

Table 4 Values of steady-state current densities of Muntz metal in sulfide-polluted artificial water in the presence and absence of the optimum concentration of PTDM, ATDA, PTAT, and ATPA at various impressed potentials

Thiadiazole derivatives	Corrosion current density values at various impressed potentials (mA cm^{-2})					
	−200 mV	−160 mV	−120 mV	−80 mV	−40 mV	0 mV
Blank	0.096	0.51	1.32	2.47	4.13	5.68
PTDM	0.041	0.19	0.47	0.91	2.04	2.79
ATDA	0.032	0.093	0.36	0.82	1.84	2.56
PTAT	0.027	0.084	0.26	0.64	1.68	2.17
ATPA	0.015	0.062	0.19	0.48	1.35	1.84

from the Tafel polarization method and the electrochemical impedance measurement; in the presence of substituted thiadiazoles, the current density values are reduced, and the corrosion of Muntz metal in sulfide-polluted artificial seawater is delayed.

3.4 Potentiodynamic polarization studies

Polarization measurements were performed on a Muntz metal electrode in sulfide-polluted artificial seawater with and without various concentrations (0.76, 1.54, 2.32, and 3.07 mM) of the four synthesized substituted thiadiazole derivatives: PTDM, ATDA, PTAT, and ATPA. Figure 5 depicts typical polarization curves displaying the optimum concentrations of the thiadiazole derivatives included in this study. Table 5 presents the electrochemical parameters, including the respective corrosion current, Tafel slopes for both the cathode and the anode, corrosion potential, and protection efficiency for Muntz metal corrosion in sulfide-polluted artificial seawater containing different concentrations of the thiadiazole derivatives under investigation. The changes in I_{corr} values with various concentrations of PTDM, ATDA, PTAT, and ATPA are shown in Fig. 5. The corrosion current density was observed to

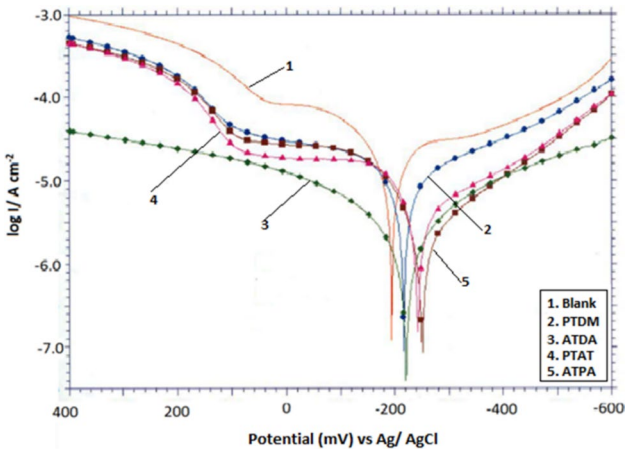

Fig. 5 Potentiodynamic polarization curves of Muntz metal in sulfide-polluted artificial seawater

decrease considerably with increasing concentrations of thiadiazole derivatives.

Table 5 shows that the corrosion current density and corrosion rate values decreased with the increasing concentration of the thiadiazole derivatives and their corresponding corrosion protection efficiencies increased, reaching the highest values at an optimum concentration of 2.32 mM. From these experimental results, all the thiadiazole derivatives employed in this test were found to decrease the corrosion current density significantly at all the concentrations assessed. Both anodic and cathodic slopes increased, indicating that the investigated thiadiazole derivatives suppressed both anodic and cathodic reactions. The thiadiazole derivatives had relatively mixed performances for Muntz metal in the chloride environment. The slight negative shifts in corrosion potential values were found at various concentrations of the substituted thiadiazoles in sulfide-polluted artificial seawater. The corrosion potential (E_{corr}) values can shift slightly because of the competing anodic and cathodic inhibitory reactions on the Muntz metal surface.

The corrosion current density values in the absence of an inhibitor were 24.09 µA cm^{-2} in sulfide-polluted artificial seawater. They were reduced by adding 2.32 mM of the thiadiazole derivatives PTDM, ATDA, PTAT, and ATPA to lower values of 2.057, 1.285, 0.909, and 0.553 µA cm^{-2}, respectively (Fig. 6).

In sulfide-polluted artificial seawater, the rate of corrosion of Muntz metal was 12.18 mils $year^{-1}$. It was reduced by adding 2.32 mM (optimum concentration) of thiadiazole derivatives PTDM, ATDA, PTAT, and ATPA to a smaller value of 1.04, 0.65, 0.46, and 0.28 mils $year^{-1}$, respectively.

The corrosion inhibition efficiency of PTDM, ATDA, PTAT, and ATPA increased with an increase in concentration up to the optimum level (2.32 mM) and some decreased afterward. In sulfide-polluted artificial seawater, the thiadiazole derivatives PTDM, ATDA, PTAT, and ATPA exhibited maximum corrosion protection efficiencies of 91.46, 94.66, 96.22, and 97.70%, respectively, at their optimum concentration. Table 5 shows the estimated corrosion resistance efficiency decreasing in the following order:

Table 5 Calculated values of polarization parameters of Muntz metal in sulfide-polluted artificial water with and without the different concentrations of thiadiazole derivatives PTDM, ATDA, PTAT, and ATPA at 303 K

Thiadiazole derivatives	Conc. of thiadiazole derivatives (mM)	−Ecorr (mV dec^{-1})	−bc (mV dec^{-1})	ba (mV dec^{-1})	Icorr (µA cm^{-2})	Rate of corrosion (mils $year^{-1}$)	Protection efficiency (%)
`	0	194	143	42	24.09	12.18	–
PTDA	0.76	204	118	73	10.31	5.21	57.22
	1.54	214	93	88	7.160	3.62	70.28
	2.32	217	82	114	2.057	1.04	91.46
	3.07	219	84	112	2.096	1.06	91.30
ATDA	0.76	207	113	79	8.624	4.36	64.20
	1.54	214	86	98	6.032	3.05	74.86
	2.32	217	72	123	1.285	0.65	94.66
	3.07	222	74	122	1.305	0.66	94.58
PTAT	0.76	236	87	86	7.971	4.03	66.91
	1.54	238	81	108	4.885	2.47	79.72
	2.32	243	59	127	0.909	0.46	96.22
	3.07	245	61	126	0.909	0.46	96.22
APTD	0.76	240	78	87	5.182	2.62	78.49
	1.54	244	63	112	3.402	1.72	85.88
	2.32	251	35	145	0.553	0.28	97.70
	3.07	252	36	142	0.593	0.30	97.54

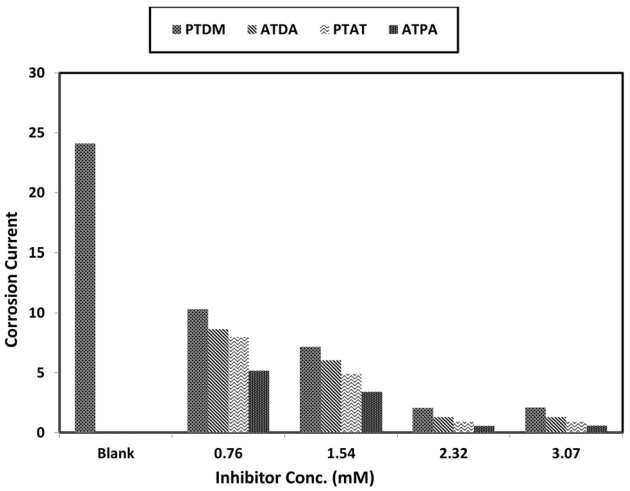

Fig. 6 Plot of corrosion current density vs. different concentrations of PTDM, ATDA, PTAT, and ATPA for Muntz metal in sulfide-polluted artificial

ATPA > PTAT > ATDA > PTDM. N-(5-phenyl-1,3,4-thiadiazol-2-yl) acetamide is the least efficient inhibitor in this study. The smaller values of corrosion inhibition efficiency for PTDM, ATDA, and PTAT compared to that of N-(5-(4-aminophenyl)-1,3,4-thiadiazole-2-yl)-2-diphenylamino) acetamide can be attributed to the reduced electron densities surrounding the chemisorption center. The better performance of ATPA over PTDM, ATDA, and PTAT is caused by the availability of more π-electrons and more surface area, which leads to more adsorption on the metal surface, thereby showing an improved protective effect [38]. Among the thiadiazole derivatives investigated, ATPA showed the maximum corrosion inhibition efficiency on the Muntz metal aqueous chloride environments. The findings of these results are consistent with the impedance measurements.

Table 6presents a comparative analysis of the inhibition efficiency (IE) of ATPA inhibitor with other thiadiazole derivatives in safeguarding brass metal. Notably, existing literature lacks corrosion investigations in sulfide-polluted seawater environments and specific mention of Muntz metal. Nevertheless, the ATPA inhibitor, utilized in this study, showcased significant inhibition efficiency in comparison to prior research.

3.5 Thermodynamic parameters

Thermodynamic data such as free energy of adsorption (ΔG_{ads}), entropy of adsorption $\left(\Delta S_{ads}\right)$, and heat of adsorption (ΔH_{ads}) are presented in Table 7 for the adsorption of substituted thiadiazole derivatives in sulfide-polluted artificial seawater on the Muntz metal surface at different temperatures. The equilibrium constant (K_{ads}) of adsorption decreased with increasing temperature, which revealed a decrease in the degree of adsorption of thiadiazole molecules on the surface of the Muntz metal. In addition, the interaction between the adsorbed thiadiazole molecules and Muntz metal surface decreased, indicating that the adsorbed thiadiazole molecules were separated. The negative value of the free energy of adsorption indicates spontaneous adsorption of the thiadiazole derivatives PTDM, ATDA, PTAT, and ATPA on the Muntz metal surface. Therefore, a strong interaction between the inhibitor molecules and alloy surface is proved to exist.

Thermodynamic parameters such as changes in Gibbs free energy (ΔG_{ads}), entropy (ΔS_{ads}), and enthalpy (ΔH_{ads}) were calculated using following thermodynamic equations:

$$G_{ads} = -RTlnb$$

$$lnb = \frac{\Delta S_{ads}}{R} - \frac{\Delta H_{ads}}{RT}$$

At standard conditions (often 25 °C or 298.15 K and 1 bar or 100 kPa), substances are assumed to be in their most stable and common forms.

The values of free energy of adsorption around −40 kJ mol^{-1} or higher correspond to chemisorption, and the free energy of adsorption up to −20 kJ mol^{-1} are associated with the electrostatic interactions between the charged molecules and the metal (physisorption), consequently representing the transfer or sharing of electrons from the organic molecules to the metal surface, forming a coordinate bond. The ΔG_{ads} values greater than −20 kJ mol^{-1} revealed that, at the optimum concentration, the thiadiazole derivatives PTDM, ATDA, PTAT, and ATPA were chemisorbed on the Muntz metal surface. Adsorption may occur first because of the significant H_2O adsorption on the alloy surface. The chemical interaction of the alloy surface with PTDM, ATDA, PTAT, and ATPA, as well as the elimination of H_2O molecules from the alloy surface resulted in chemisorption.

The negative values of the free energy of adsorption show spontaneous adsorption of the investigated thiadiazole derivatives on the Muntz metal surface at different temperatures (303, 318, 333, 348, and 363 K). The ΔG_{ads} values represent chemical adsorption in nature. The free energy of adsorption decreased negatively with the increase in temperature, indicating desorption of the investigated thiadiazole derivatives. When the temperature increased, there was a slight decrease in the free energy of adsorption values, indicating that adsorption is unfavorable at a higher temperature for both physical and chemical adsorption.

The heat of adsorption values at the optimum concentration (2.32 mM) of thiadiazole derivatives in sulfide-polluted artificial seawater was determined by plotting $\ln K_{ads}$ versus 1/T, and straight lines were obtained with a slope equal to $(-\Delta H_{ads}/RT)$, as shown in Fig. 7.

Generally, an endothermic process is specific to chemical adsorption, whereas an exothermic process is specific

Table 6 Lists the comparison of IE with other thiadiazole derivatives inhibitors protecting brass metal

Inhibitors	Alloy	IE (%)	Medium	References
Thiadiazole derivatives, namely, 2-amino-5-(4-methoxyphenyl)-1,3,4-thiadiazole (AMOPTD), 2-amino-5-(4-methylphenyl)-1,3,4-thiadiazole (AMPTD), 2-amino-5-(4-pyridinyl)-1,3,4-thiadiazole (APTD), and 2-amino-5-(4-nitrophenyl)-1,3,4-thiadiazole (ANPTD)	Brass (65.3% Cu,34.44% Zn, 0.1385% Fe, and 0.0635% Sn)	97.1 (AMOPTD)	Natural Seawater	[39]
salicylaldoxime and 4(5)-methylimidazole	brass (Cu37Zn)	98.3	3% NaCl	[3]
2,5-bis(ethyldisulfanyl)-1,3,4-thiadiazole (DTA), dimercapto1,3,4-thiadiazole (DMDT)	Cu–O (92 Cu atoms, 16 O atoms)	93.78 (DTA)	lubricating oil	[40]
2-Amino-1,3,4-thiadiazole (ATD), 2-Amino-5-methyl-1,3,4- thiadiazole (AMTD) and 2-Amino-5-methyl-thio-1,3,4-thiadiazole (AMTTD)	65–35 brass	89	natural seawater	[41]
1-(prop-2-yn-1-yl)-1H-benzotriazole(Inh1),2-[2-(1H-benzotriazol-1-yl) ethyl]-1H-isoindole-1,3(2H)-dione(Inh2) and1-(4-nitrobenzyl)-1H-1,2,3-benzotriazole (Inh3)	Brass (C68700)	92.13 (Inh3)	3% NaCl	[42]
2,5-bis(n-methylphenyl)-1,3,4-oxadiazole	Brass (58Cu–40Zn–2Pb)	91	cooling water	[43]
2-amino-5-ethyl-1,3,4-thiadiazole (AETD)	Brass (Cu37Zn)	93.1	3% NaCl	[44]
2-(5-methyl-2-nitro-1H-imidazol-1-yl)ethyl benzoate (IMDZ-B)	34.20% of Cu, 62.66% of Zn, 2.89% of Pb, 0.12% of Fe, 0.069% of Ni, and 0.057% of P	91.02%	0.5-M H_2SO_4	[45]
5-phenyl-1H-tetrazole(PTAH)and 5-(4-pyridyl)-1H-tetrazole(PyTAH)	brass(61.76-wt% Cu, 36.28-wt% Zn, 1.13-wt% Al, 0.4-wt% Fe, and 0.43-wt% Ni)	96.27%	3.5% NaCl	[46]
3-mercaptopropyl-5-amino-1H-1,2,4-triazole (inhibitor A), 3-mercaptobutyl-5-amino-1H-1,2,4-triazole (inhibitor B), and 3-mercapto(3-methylbutyl)-5-amino-1H-1,2,4-triazole (inhibitor C)	α-brass (Cu/Zn: 63/37)	99.8% (inhibitor A),	10-mM NaCl	[47]
2,5-bis-(4-aminophenyl)-1,3,4-oxadiazole (BAPOD), 2,5-bis-(4-bromophenyl)-1,3,4-oxadiazole (BBPOD), 2,5-diphenyl-1,3,4-oxadiazole (DPOD), and 2,5-bis-(4-nitrophenyl)-1,3,4-oxadiazole (BNPOD)	brass (s wt% 65.3 Cu, 34.44 Zn, 0.1385 Fe, and 0.0635 Sn)	87% (BAPOD)	natural seawater	[48]
N-(5-phenyl-1,3,4-thiadiazol-2-yl)acetamide (PTDM), N-(5-(4-aminophenyl)-1,3,4-thiadiazole-2-yl)-2-(diethylamino) acetamide (ATDA), 2-(5-phenyl-1,3,4-thiadiazol-2-ylamino)-N-p-tolyl acetamide (PTAT) and N-(5-(4-aminophenyl)-1,3,4-thiadiazole-2-yl)-2-diphenylamino)acetamide (ATPA)	Muntz metal (60Cu-40Zn)	97.70 (ATPA)	Sulfide-polluted artificial seawater	This work

to either physical or chemical adsorption. In exothermic adsorption, the specific type is based on the absolute heat value of adsorption. If the enthalpy of adsorption value is less than −40 kJ mol^{-1}, it indicates physical adsorption, and values above −40 kJ mol^{-1} represent chemisorption. It is evident from the table that the adsorption is an exothermic process [49]. Here, the obtained enthalpy values of the investigated thiadiazole derivatives were higher than 40 kJ mol^{-1}, confirming chemisorption. The negative values of ΔS_{ads} on the inhibitor in the adsorption process are explained as follows: thiadiazole molecules are adsorbed in an orderly manner on the Muntz metal surface, resulting in a decrease in the entropy of the system.

Adsorption isotherm

The amount of surface covered (θ) was calculated at varying concentrations of thiadiazole derivatives PTDM, ATDA, PTAT, and ATPA and were plotted graphically so that, whether they fitted with the Langmuir. And we obtained a

Table 7 Values of thermodynamic parameters for the adsorption of thiadiazoles PTDM, ATDA, PTAT, and ATPA on the Muntz metal surface in sulfide-polluted artificial seawater from 303 to 363 K

Thiadiazole derivatives	Temp (K)	Kads ($dm^3\ mol^{-1}$)	$-\Delta$Gads (KJ mol^{-1})	$-\Delta$Hads (KJ mol^{-1})	$-\Delta$Sads (J $mol^{-1}\ K^{-1}$)
PTDM	303	6327	32.17	44.43	40.46
	318	5283	33.29	44.43	35.03
	333	4628	34.49	44.43	29.86
	348	4103	35.70	44.43	25.09
	363	3576	36.82	44.43	20.96
ATDA	303	7253	32.52	46.94	47.59
	318	5854	33.44	46.94	42.45
	333	5153	34.79	46.94	36.49
	348	4457	35.94	46.94	31.61
	363	4063	37.20	46.94	26.83
PTAT	303	9635	33.23	49.13	52.48
	318	8842	34.65	49.13	45.53
	333	8536	36.19	49.13	38.86
	348	8195	37.70	49.13	32.84
	363	7753	39.15	49.13	27.49
ATPA	303	12,547	33.90	51.58	58.35
	318	11,443	35.33	51.58	51.10
	333	11,061	36.90	51.58	44.08
	348	10,783	38.49	51.58	37.61
	363	10,429	40.05	51.58	31.76

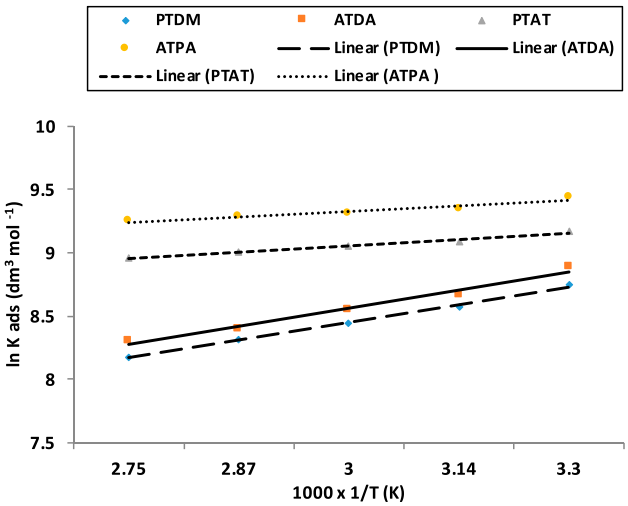

Fig. 7 Adsorption isotherm plots for PTDM, ATDA, PTAT, and ATPA in sulfide-polluted artificial seawater

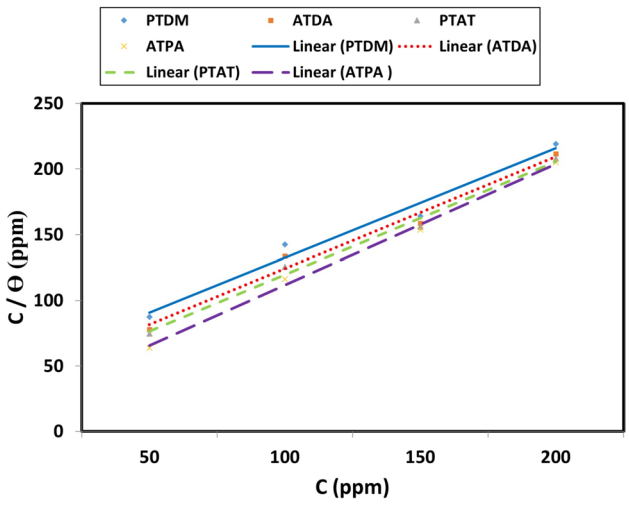

Fig. 8 Langmuir adsorption isotherm for different concentrations of PTDM, ATDA, PTAT, and ATPA adsorbed on Muntz metal surface in sulfide-polluted artificial sea water

straight line in Fig. 8 indicating that adsorption follows the Langmuir adsorption isotherm. The values of free energy of adsorption for thiadiazole derivatives PTDM, ATDA, PTAT, and ATPA are calculated from the Langmuir-type adsorption isotherm in sulfide-polluted artificial sea water. The negative value of free energy of adsorption (ΔGads) denotes spontaneous adsorption of the thiadiazole molecules on the Muntz metal surface and also the effective interaction between thiadiazole molecules and the Muntz metal surface. Generally, the values of free energy of adsorption (ΔGads) below -20 kJ/mol are consistent with electrostatic interaction (physical adsorption), while those above -20 kJ/mol represents chemisorption. The value of ΔG_ads for all thiadiazole derivatives PTDM, ATDA, PTAT and ATPA points to the spontaneity of the adsorption process under investigated experimental conditions and it also points out that the

adsorption of thiadiazole derivatives occurs predominantly by chemisorption.

3.6 Accelerated leaching studies by ICP-AES

The results of accelerated leaching studies and the corresponding dezincification index (z), in the absence and presence of different concentrations of the substituted thiadiazoles PTDM, ATDA, PTAT, and ATPA in sulfide-polluted artificial seawater, are given in Table 8. Figure 9 shows the effect of different concentrations of the thiadiazole derivatives PTDM, ATDA, PTAT, and ATPA on the dissolution of Muntz metal in sulfide-polluted artificial seawater. The findings confirmed that the concentrations of Zn and Cu released from the alloy decreased with increasing concentrations of thiadiazole derivatives, and the corrosion inhibition efficiency (%) increased with increasing concentrations of thiadiazoles, attaining the highest value at 2.32 mM of

Table 8 Effect of different concentrations of substituted thiadiazoles PTDM, ATDA, PTAT, and ATPA on the dezincification of Muntz metal in sulfide-polluted artificial water

Thiadiazole derivatives	Conc. of thiadiazole derivatives (mM)	Conc. of ions (ppm)		Dezincification index (z)	Inhibition efficiency (%)	
		Zinc	Copper		Zinc	Copper
Blank	0	13.56	0.938	22.08	–	–
PTDM	0.76	5.67	0.335	25.85	58.19	64.29
	1.54	2.72	0.192	21.64	79.94	79.53
	2.32	0.83	0.063	20.12	93.88	93.28
	3.07	0.85	0.065	19.97	93.73	93.07
ATDA	0.76	5.24	0.306	26.16	61.36	67.38
	1.54	2.38	0.146	24.90	82.45	84.43
	2.32	0.71	0.052	20.86	94.76	94.46
	3.07	0.73	0.054	20.65	94.61	94.24
PTAT	0.76	4.69	0.262	27.34	65.41	72.06
	1.54	2.02	0.112	27.55	85.10	88.06
	2.32	0.46	0.039	18.02	96.61	95.84
	3.07	0.47	0.041	17.51	96.53	95.63
ATPA	0.76	4.06	0.216	28.71	70.06	76.97
	1.54	1.47	0.074	30.34	89.16	92.11
	2.32	0.23	0.026	13.51	98.30	97.23
	3.07	0.25	0.027	14.14	98.16	97.12

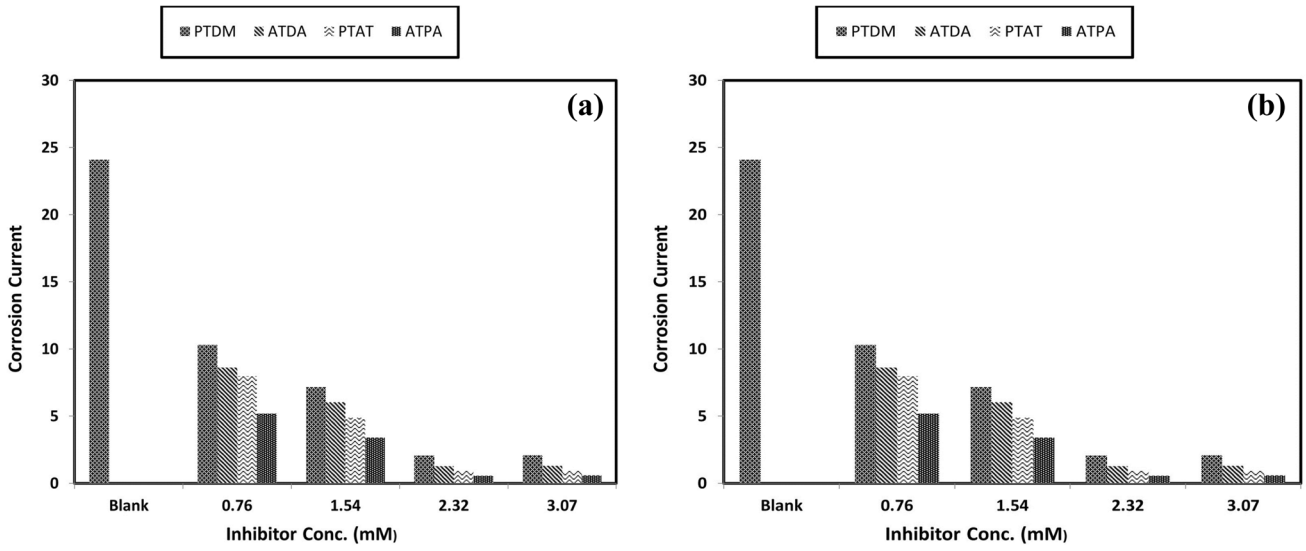

Fig. 9 Amount of **a** Cu and **b** Zn released from Muntz metal in sulfide-polluted artificial seawater with different quantities of PTDM, ATDA, PTAT, and ATPA

inhibitor concentration. This corresponds to the development of a stable metal-thiadiazole layer on the surface of the Muntz metal, which acts as a barrier between the alloy and the corrosive medium, preventing the bare metal from making contact with the solution.

The amount of zinc ions released from the Muntz metal in the absence of the thiadiazole derivatives in sulfide-polluted artificial seawater was 13.56 ppm. The amount of zinc ions leached was decreased by increasing the concentration of the thiadiazole derivatives.

In sulfide-polluted artificial seawater, the thiadiazole derivatives PTDM, ATDA, PTAT, and ATPA showed a significantly lower tendency to leach out the zinc ions at 0.83, 0.71, 0.46, and 0.23 ppm, at their optimum concentrations. The thiadiazole derivatives PTDM, ATDA, PTAT, and ATPA also showed their highest corrosion protection efficiencies of 93.88, 94.76, 96.61, and 98.30%, respectively, at their optimum concentration. Among the thiadiazole derivatives examined, ATPA revealed the highest corrosion inhibition efficiency on the Muntz metal in aqueous sulfide-polluted artificial seawater.

Similarly, the amount of copper ions leached from the Muntz metal in the absence of thiadiazole derivatives in sulfide-polluted artificial seawater was 0.938 ppm. The amount of copper ions leached decreased by increasing the concentration of thiadiazole derivatives. In sulfide-polluted artificial seawater, the thiadiazole derivatives PTDM, ATDA, PTAT, and ATPA tended to leach out the copper ions at 0.063, 0.052, 0.039, and 0.026 ppm less at their optimum concentrations. In sulfide-polluted artificial seawater, the thiadiazole derivatives PTDM, ATDA, PTAT, and ATPA showed the highest corrosion protection efficiencies of 93.28, 94.46, 95.84, and 97.23%, respectively, at their optimum concentration. Among the four thiadiazole derivatives examined, ATPA showed the highest corrosion inhibition efficiency for Muntz metal in a chloride environment. The dezincification index value of 14.14 for Muntz metal was attained with the help of ATPA-containing sulfide-polluted artificial seawater. The higher zinc content in the solution during dezincification is due to the preferential corrosion and dissolution of zinc, driven by the electrochemical potential difference between copper and zinc, as well as the greater mobility and easier diffusion of zinc atoms from the beta phase (BCC) compared to the alpha phase (FCC). ATPA achieved the highest inhibition efficiency against the dissolution of zinc in the solution, that is, 98.30% for Muntz metal, indicating that the preferential dissolution of zinc was almost completely minimized. The order of the four inhibitors, by the amounts of Cu and Zn released from the Muntz metal in their presence is as follows: PTDM > ATDA > PTAT > ATPA. These findings are in excellent agreement with the weight loss and electroanalytical techniques.

3.7 Scanning electron microscopy (SEM) and energy-dispersive X-ray analysis

Scanning electron microscopy studies provide supplementary information on the growth of inhibitive films on metal and alloy surfaces. To study the performance of the thiadiazole derivatives PTDM, ATDA, PTAT, and ATPA, SEM analysis was carried out after the immersion of the Muntz metal in samples of sulfide-polluted artificial seawater containing the optimum concentration of inhibitor for approximately 5 days. SEM micrographs of the Muntz metal in the absence and presence of substituted thiadiazoles are shown in Fig. 9. In this figure, (a) illustrates the scanning electron micrographs of the Muntz metal in sulfide-polluted artificial seawater without thiadiazole derivatives and conveys that the surface was found to be severely damaged. Cracks and pits were observed on the corroded Muntz metal surface. The aggressive chloride ions present in the sulfide-polluted artificial seawater violently counteracted the Muntz metal; hence, the surface was highly corroded. Figure 9b–e shows the scanning electron micrographs of the Muntz metal surface in sulfide-polluted artificial seawater in the presence of substituted thiadiazoles PTDM, ATDA, PTAT, and ATPA. The surface was found covered in a protective coating of metal (copper and zinc)-thiadiazole complexes, which controlled the dissolution of copper and zinc. The metal-thiadiazole complex layer has less permeability and better strength than the unprotected Muntz metal surface. Thus, the surface exhibited superior properties and provided corrosion protection to the Muntz metal surface. Furthermore, the width of the inhibitive film increased; therefore, the corrosion protection also increased.

Thiadiazole molecules have a strong tendency to adhere to Muntz metal surfaces. Thiadiazole molecules adsorb on the Muntz metal surface by sharing electrons between the nitrogen and copper atoms. This observation confirms that the protection is due to the development of a layer during the adsorption of heterocyclic organic molecules on the Muntz metal surface. The thiadiazole derivatives were clearly modified, perhaps because of chemisorption on the oxidized metal surface. The chemisorption of the thiadiazole molecules on the metal surface could occur directly via donor–acceptor interactions between the π electrons of the heterocyclic compound and the vacant d-orbitals of the copper surface or the interaction of thiadiazole with the already adsorbed chloride ions [25].

EDX analysis was carried out on the Muntz metal surface in sulfide-polluted artificial seawater containing the optimum concentration of thiadiazole derivatives PTDM, ATDA, PTAT, and ATPA. The EDX spectra are shown in Fig. 10. An energy-dispersive X-ray spectrum was employed to determine the elements present on the Muntz metal surface, before and after exposure to the thiadiazole derivatives

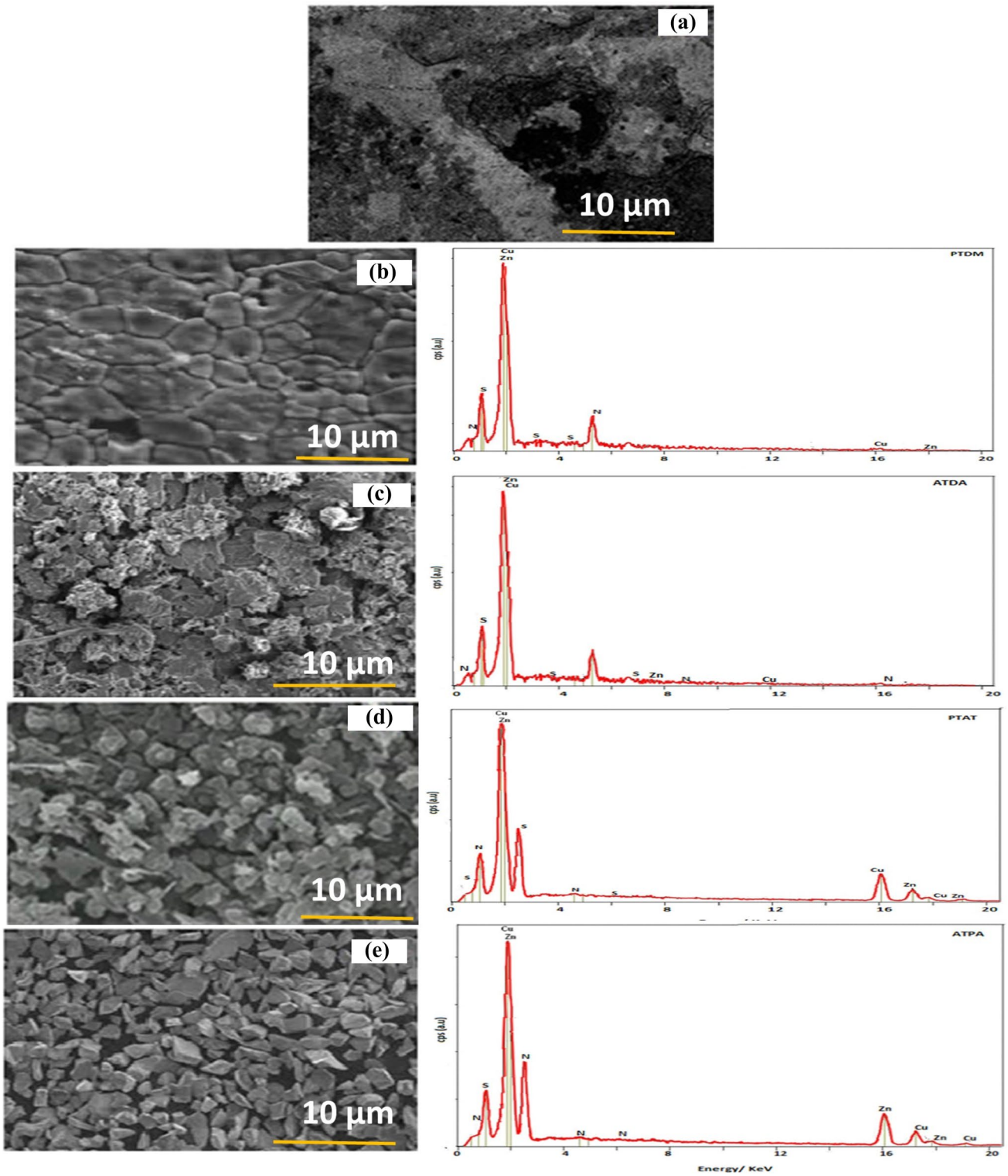

Fig. 10 SEM and respective EDX spectra of the Muntz metal surface in sulfide-polluted artificial seawater containing optimum concentrations of **a** blank, **b** PTDM, **c** ATDA, **d** PTAT, and **e** ATPA

in sulfide-polluted artificial seawater solution. Only Zn, Cu, Cl, and O peaks appeared in the EDX spectra of the sulfide-polluted artificial seawater without thiadiazole derivatives, and this is due to the formation of Cu_2O and ZnO, Cu_2S, and ZnS. The absence of chlorine atoms in the spectra also confirms the capacity of PTDM, ATDA, PTAT, and ATPA

molecules to prevent the formation of copper chloride and oxychloride complexes, suggesting that the corrosion was competently controlled in their presence. However, in the presence of the optimum concentration (2.32 mM) of the thiadiazole derivatives PTDM, ATDA, PTAT, and ATPA, nitrogen and sulfur atoms were observed, and these atoms coordinated with the Muntz metal surface, thus forming copper and zinc complexes of the thiadiazoles, preventing the corrosion of the metal surface. This illustrates that the thiadiazole molecules were adsorbed on the copper–zinc alloy surface and formed a thin, and very adherent, protective film on the metal surface in all cases, which is accountable for the corrosion protection of the metal in sulfide-polluted artificial seawater.

4 Conclusion

The impact of thiadiazole derivatives on the corrosion behavior of the Muntz metal (brass) alloy was evaluated in sulfide-polluted artificial seawater. The inhibition efficiency was found to increase with increasing concentrations of all inhibitors. In the chemical method, the weight loss and corrosion rate decreased appreciably with increasing concentrations of azole derivatives. With potentiodynamic polarization techniques, the corrosion inhibition efficiency increased, and the corrosion current (I_{corr}) and corrosion rate decreased with increasing concentrations of thiadiazoles. Electrochemical impedance indicated that the charge transfer resistance became dominant in the corrosion process owing to the formation of an inhibitor film on the alloy surface. Potentiostatic current–time transient techniques revealed that the thiadiazole derivatives included in the study decreased the steady-state current density values of the Muntz metal alloy. Thus, the azole derivatives reduced the corrosion rate and efficiently controlled the dissolution of Cu and Zn in sulfide-polluted artificial seawater. The corrosion inhibition efficiency also decreased with increasing solution temperature at the optimum concentration of the azole derivatives. The SEM and EDX analyses confirmed that the corrosion protection process was associated with the development of a protective film on the metal and alloy surfaces. Electrochemical and surface characterization techniques proved to be successful in describing the better protective effect of organic compounds on the corrosion of Muntz metal in a neutral aqueous chloride environment.

Supplementary Information The online version contains supplementary material available at https://doi.org/10.1007/s10800-023-02009-4.

Acknowledgements The authors extend their thanks to Researchers Supporting Project (Ref: RSPD2023R670), King Saud University, Riyadh, Saudi Arabia.

Author contributions PR, SK, and JKA conceived the project; PS, IH, JM, and SA, performed the experiments, generated datasets, and wrote the first draft of the manuscript; IH, SA, AKY, and YHA supervised the project and edited and revised the manuscript. All authors have read and agreed to the published version of the manuscript.

Data availability No data were used for the research described in this article.

Declarations

Conflict of interest The authors declare that they have no competing interests.

Informed consent Informed consent was obtained from all the subjects involved in the study.

Institutional review board Not applicable.

References

1. Scendo M (2007) Corrosion inhibition of copper by purine or adenine in sulphate solutions. Corros Sci 49:3953–3968. https://doi.org/10.1016/j.corsci.2007.03.037
2. Scendo M (2008) Inhibition of copper corrosion in sodium nitrate solutions with nontoxic inhibitors. Corros Sci 50:1584–1592. https://doi.org/10.1016/j.corsci.2008.02.015
3. Radovanović MB, Tasić ŽZ, Mihajlović MBP, Simonović AT, Antonijević MM (2019) Electrochemical and DFT studies of brass corrosion inhibition in 3% NaCl in the presence of environmentally friendly compounds. Sci Rep 9:1–16. https://doi.org/10.1038/s41598-019-52635-2
4. Kosec T, Milošev I, Pihlar B (2007) Benzotriazole as an inhibitor of brass corrosion in chloride solution. Appl Surf Sci 253:8863–8873. https://doi.org/10.1016/j.apsusc.2007.04.083
5. Antonijevic M, Milic S, Radovanovic M, Petrovic M, Stamenkovic A (2009) Influence of pH and chlorides on electrochemical behavior of brass in presence of benzotriazole. Int J Electrochem Sci 4:1719–1734
6. Brandt MJ, Johnson KM, Elphinston AJ, Ratnayaka DD (2017) Chapter 10 - specialized and advanced water treatment processes. In: Brandt MJ, Johnson KM, Elphinston AJ, Ratnayaka DD (eds) Twort's water supply, 7th edn. Butterworth-Heinemann, Boston, pp 407–473
7. Brock J (2001) Copper alloys: corrosion. In: Buschow KHJ, Cahn RW, Flemings MC, Ilschner B, Kramer EJ, Mahajan S, Veyssière P (eds) Encyclopedia of materials: science and technology. Elsevier, Oxford, pp 1662–1664
8. Karpagavalli R, Balasubramaniam R (2007) Development of novel brasses to resist dezincification. Corros Sci 49:963–979. https://doi.org/10.1016/j.corsci.2006.06.024
9. Sohn S, Kang T (2002) The effects of tin and nickel on the corrosion behavior of 60Cu–40Zn alloys. J Alloy Compd 335:281–289. https://doi.org/10.1016/S0925-8388(01)01839-4
10. Ravichandran R, Nanjundan S, Rajendran N (2004) Effect of benzotriazole derivatives on the corrosion and dezincification of brass in neutral chloride solution. J Appl Electrochem 34:1171–1176
11. Drach A, Tsukrov I, DeCew J, Aufrecht J, Grohbauer A, Hofmann U (2013) Field studies of corrosion behaviour of copper alloys in natural seawater. Corros Sci 76:453–464
12. Tabish M, Wang J, Qiang Y, Yan J, Kumar A, Yasin G (2022) Organocerium/Ce-based nanocomposites as corrosion inhibitors. In: Functionalized nanomaterials for corrosion mitigation:

synthesis, characterization, and applications, American Chemical Society, pp. 169–188
13. Rani BEA, Basu BBJ (2012) Green inhibitors for corrosion protection of metals and alloys: an overview. Int J Corros. https://doi.org/10.1155/2012/380217
14. Ramji K, Cairns DR, Rajeswari S (2008) Synergistic inhibition effect of 2-mercaptobenzothiazole and Tween-80 on the corrosion of brass in NaCl solution. Appl Surf Sci 254:4483–4493. https://doi.org/10.1016/j.apsusc.2008.01.031
15. Shahnawaz M, Muhammad N (2021) Surface characterisation of brass alloy in the correlation of hardness and electrical resistivity by carbon ion implantation. Mater Sci Technol 37:1483–1495
16. Sherif E, Park SM (2006) Effects of 2-amino-5-ethylthio-1, 3, 4-thiadiazole on copper corrosion as a corrosion inhibitor in aerated acidic pickling solutions. Electrochim Acta 51:6556–6562. https://doi.org/10.1080/02670836.2021.2017659
17. Lalitha A, Ramesh S, Rajeswari S (2005) Surface protection of copper in acid medium by azoles and surfactants. Electrochim Acta 51:47–55
18. Bartley J, Huynh N, Bottle S, Flitt H, Notoya T, Schweinsberg D (2003) Computer simulation of the corrosion inhibition of copper in acidic solution by alkyl esters of 5-carboxybenzotriazole. Corros Sci 45:81–96
19. Berchmans LJ, Sivan V, Iyer SVK (2006) Studies on triazole derivatives as inhibitors for the corrosion of muntz metal in acidic and neutral solutions. Mater Chem Phys 98:395–400
20. Lokesh S, Satpati A, Sherigara B (2010) Electrochemical behavior of 1, 2, 4-triazole and benzotriazole at glassy carbon electrode in acidic media. Open Electrochem J 2:15–21
21. Satpati A, Ravindran P (2008) Electrochemical study of the inhibition of corrosion of stainless steel by 1,2,3-benzotriazole in acidic media. Mater Chem Phys 109:352–359
22. El Attari H, El Bribri A, Mhaidra L, Bentiss F, Siniti M (2015) Synthesis and anticorrosion for carbon steel of 4-amino-3,5 bis (4-hydroxy-3-methoxy)-1,2,4-triazole in hydrochloric acid solution. Am J Eng Res 4:44–51
23. Zhang W, Li C, Wang W, Li B, Liu X, Liu Y, Guo H, Chen S, Feng Y (2022) Laminarin and sodium molybdate as efficient sustain able inhibitor for Q235 steel in sodium chloride solution. Colloids Surf A 637:128199
24. Zhang W, Nie B, Wang M, Shi S, Gong L, Gong W, Pang H, Liu X, Li B, Feng Y (2021) Chemically modified resveratrol as green corrosion inhibitor for Q235 steel: electrochemical, SEM, UV and DFT studies. J Mol Liq 343:117672
25. Bentiss F, Traisnel M, Lagrenee M (2001) Influence of 2,5-bis (4-dimethylaminophenyl)-1,3,4-thiadiazole on corrosion inhibition of mild steel in acidic media. J Appl Electrochem 31:41–48
26. Sastri VS (1998) Corrosion inhibitors: principles and applications. Wiley, New York
27. Bentiss F, Lagrenée M, Traisnel M (2000) 2,5-bis (n-pyridyl)-1,3,4-oxadiazoles as corrosion inhibitors for mild steel in acidic media. Corrosion 56(7):733–742
28. Rahim AA, Rocca E, Steinmetz J, Kassim MJ, Adnan R, Ibrahim MS (2007) Mangrove tannins and their flavanoid monomers as alternative steel corrosion inhibitors in acidic medium. Corros Sci 49:402–417
29. Zhang QH, Hou BS, Zhang GA (2020) Inhibitive and adsorption behavior of thiadiazole derivatives on carbon steel corrosion in CO_2-saturated oilfield produced water: effect of substituent group on efficiency. J Colloid Interface Sci 572:91–106
30. Ravichandran R, Rajendran N (2005) Electrochemical behaviour of brass in artificial seawater: effect of organic inhibitors. Appl Surf Sci 241:449–458
31. Sharshira EM, Hamada NMM (2012) Synthesis and antimicrobial evaluation of some pyrazole derivatives. Molecules 17:4962–4971
32. Rao M (2017) Dielectric studies on PVA/PVP: go based nanocomposite polymer films. Chem Sci Rev Lett 6:832–837
33. Bentiss F, Traisnel M, Gengembre L, Lagrenée M (2000) Inhibition of acidic corrosion of mild steel by 3,5-diphenyl-4H-1,2,4-triazole. Appl Surf Sci 161:194–202
34. Ramesh S, Rajeswari S, Maruthamuthu S (2004) Corrosion inhibition of copper by new triazole phosphonate derivatives. Appl Surf Sci 229:214–225
35. Bengough GD, May R (1924) Seventh report to the corrosion research committee of the institute of metals. J Inst Metals 32:81
36. Jones D (1992) Principles and prevention of corrosion. Macmillan, New York, p 568
37. Abbas M (1991) Effects of temperature on dezincification and electrochemical behaviour of 70–30 brass in sulphuric acid. Br Corros J 26:273–278
38. Wang HL, Liu RB, Xin J (2004) Inhibiting effects of some mercapto-triazole derivatives on the corrosion of mild steel in 1.0 M HCl medium. Corros Sci 46:2455–2466
39. Xavier JR, Nanjundan S, Rajendran N (2012) Electrochemical adsorption properties and inhibition of brass corrosion in natural seawater by thiadiazole derivatives: experimental and theoretical investigation. Ind Eng Chem Res 51:30–43
40. Xiong S, Liang D, Ba Z, Zhang Z, Luo S (2019) Adsorption behavior of thiadiazole derivatives as anticorrosion additives on copper oxide surface: computational and experimental studies. Appl Surf Sci 492:399–406
41. Raj XJ, Rajendran N (2014) Effect of thiadiazole derivatives on the corrosion of brass in natural seawater by electrochemical techniques. J Mater Environ Sci 5(1):215–224
42. Souad B, Chafia S, Hamza A, Wahiba M, Issam B (2021) Synthesis, experimental and DFT studies of some benzotriazole derivatives as brass C68700 corrosion inhibitors in NaCl 3%. ChemSelect 6:1378–1384
43. Rochdi A, Kassou O, Dkhireche N, Touir R, El Bakri M, Touhami ME, Sfaira M, Mernari B, Hammouti B (2014) Inhibitive properties of 2,5-bis (n-methylphenyl)-1,3,4-oxadiazole and biocide on corrosion, biocorrosion and scaling controls of brass in simulated cooling water. Corros Sci 80:442–452
44. Radovanović M, Mihajlović MP, Antonijević M (2016) 2-Amino-5-ethyl-13, 4-thiadiazole as inhibitor of brass corrosion in 3% NaCl. Metall Mater Eng 22:51–60
45. Khrifou R, Touir R, Koulou A, El Bakri H, Rbaa M, Touhami ME, Zarrouk A, Benhiba F (2021) The influence of low concentration of 2-(5-methyl-2-nitro-1H-imidazol-1-yl) ethyl benzoate on corrosion brass in 0.5 M H_2SO_4 solution. Surf Interfaces 24:101088
46. Mahdy SA, Abdel-Gawad SA, El-Sherif RM, Ghayad I (2023) Corrosion inhibition on copper and commercial brass in simulated seawater using 5-Phenyl-1 H-tetrazole and 5-(4-Pyridyl)-1 H-tetrazole. Ind Eng Chem Res 62:11784–11794
47. Kozaderov O, Shikhaliev K, Prabhakar C, Tripathi A, Shevtsov D, Kruzhilin A, Komarova E, Potapov A, Zartsyn I, Kuznetsov Y (2019) Corrosion of α-brass in solutions containing chloride ions and 3-Mercaptoalkyl-5-amino-1 H-1, 2, 4-triazoles. Appl Sci 9:2821
48. Joseph Raj X, Rajendran N (2012) Effect of some oxadiazole derivatives on the corrosion inhibition of brass in natural seawater. J Mater Eng Perform 21:1363–1373
49. Torres-Knoop A, Poursaeidesfahani A, Vlugt TJH, Dubbeldam D (2017) Behavior of the enthalpy of adsorption in nanoporous materials close to saturation conditions. J Chem Theory Comput 13:3326–3339